Low-Threshold Coherent Emission at 1.5 µm from Fully Er3+ Doped Monolithic 1D Dielectric Microcavity Fabricated Using Radio Frequency Sputtering

ceramics

MDPI

Article

Low-Threshold Coherent Emission at 1.5 μm from Fully Er^{3+} Doped Monolithic 1D Dielectric Microcavity Fabricated Using Radio Frequency Sputtering

Cesare Meroni [1,2], Francesco Scotognella [3,4], Yann Boucher [5], Anna Lukowiak [6], Davor Ristic [7], Giorgio Speranza [1,8], Stefano Varas [1], Lidia Zur [1,9], Mile Ivanda [7], Stefano Taccheo [10], Roberta Ramponi [11], Giancarlo C. Righini [9,12], Maurizio Ferrari [1,9] and Alessandro Chiasera [1,*]

1 Institute for Photonics and Nanotechnologies IFN -National Research Council CNR CSMFO Lab. & Fondazione Bruno Kessler FBK—Centro Materiali e Microsistemi CMM, via alla Cascata 56/C Povo, 38123 Trento, Italy; cesare.meroni@studenti.unitn.it (C.M.); speranza@fbk.eu (G.S.); stefano.varas@ifn.cnr.it (S.V.); zur@fbk.eu (L.Z.); maurizio.ferrari@cnr.ifn.it (M.F.)
2 Dipartimento di Fisica, Università di Trento, via Sommarive 14, Povo, 38123 Trento, Italy
3 Politecnico di Milano, Dipartimento di Fisica and Institute for Photonics and Nanotechnologies IFN—National Research Council CNR, Piazza Leonardo da Vinci 32, 20133 Milano, Italy; francesco.scotognella@polimi.it
4 Center for Nano Science and Technology@PoliMi, Istituto Italiano di Tecnologia, Via Giovanni Pascoli, 70/3, 20133 Milan, Italy
5 Laboratoire FOTON (National Center for Scientific Research- Mixed Research Unit UMR CNRS 6082) Équipe Systèmes Photoniques, ENSSAT, CS 80518, F-22305 Lannion, France; boucher@enib.fr
6 Institute of Low Temperature and Structure Research, PAS, 2 Okolna St., 50-422 Wroclaw, Poland; a.lukowiak@intibs.pl
7 Center of Excellence for Advanced Materials and Sensing Devices, Ruđer Bošković Institute, Bijenička c. 54, 10000 Zagreb SA1 8EN, Croatia; Davor.Ristic@irb.hr (D.R.); ivanda@irb.hr (M.I.)
8 Fondazione Bruno Kessler-FBK Centro Materiali e Microsistemi CMM Functional Materials and Photonics Structures FMPS Unit, via Sommarive 18, Povo, 38123 Trento, Italy
9 Enrico Fermi Center, Piazza del Viminale 1, 00184 Roma, Italy; giancarlo.righini@centrofermi.it
10 College of Engineering, Swansea University, Singleton Park, Swansea SA1 8EN, UK; S.Taccheo@swansea.ac.uk
11 Institute for Photonics and Nanotechnologies IFN—National Research Council CNR and Politecnico di Milano, Dipartimento di Fisica, Piazza Leonardo da Vinci 32, 20133 Milano, Italy; roberta.ramponi@polimi.it
12 MiPLab. "Nello Carrara" Institute of Applied Physics IFAC—National Research Council CNR, Via Madonna del Piano 10, 50019 Sesto Fiorentino, Italy
* Correspondence: alessandro.chiasera@ifn.cnr.it; Tel.: +39-046-131-4923

Received: 17 December 2018; Accepted: 18 January 2019; Published: 21 January 2019

Abstract: Low threshold coherent emission at 1.5 μm is achieved using Er^{3+}-doped dielectric 1D microcavities fabricated with a Radio Frequency-sputtering technique. The microcavities are composed of a half-wavelength Er^{3+}-doped SiO_2 active layer inserted between two Bragg reflectors consisting of ten, five, and seven pairs of SiO_2/TiO_2 layers, also doped with Er^{3+} ions. The morphology of the structure is inspected using scanning electron microscopy. Transmission measurements show the third and first order cavity resonance at 530 nm and 1.5 μm, respectively. The photoluminescence measurements are obtained using the optical excitation at the third order cavity resonance using a 514.5 nm Ar^+ laser or Xe excitation lamp at 514.5 nm, with an excitation angle of 30°. The full width at half maximum of the emission peak at 1535 nm decreased with the pump power until the spectral resolution of the detection system was 2.7 nm. Moreover, the emission intensity presents a non-linear behavior with the pump power and a threshold at about 4 μW.

Keywords: 1D photonic crystals; RF-sputtering; coherent emission; erbium; silica; titania

1. Introduction

Glasses are the basis for the development of many devices in optical communication, and the possibility to be activated with lanthanide ions allows for the realization of optical amplifiers and light sources [1,2]. The advantages in using glasses, and in particular oxide-based dielectric materials, are related to their wide transparency from the ultraviolet to the near-infrared, and good resistance to temperature, corrosion, and radiation [3–5]. These features make glass materials particularly convenient for fabricating active optically-confined structures. In the last few years, a lot of effort has been directed in developing appropriate material systems and configurations to exploit and enhance the best luminescence properties of lanthanide ions, such as Er^{3+} ions, in photonic glasses [6,7]. A possibility for enhancing the emission properties of emitters is given by tailoring their surroundings [8,9]. With this aim, several approaches using nanocomposite materials or specific geometries, such as planar interfaces, photonic crystals, solid state planar microcavities, dielectric nanospheres, and spherical microresonators, have been proposed. Moreover, when only Er^{3+} ions are present in compact systems, the pumping scheme of the structure becomes crucial, since the Er^{3+} absorption cross-sections are not sufficiently high. To alleviate this issue, various configurations are proposed in the literature, such as the addition of sensitized ions of nanoparticles [10–13].

Among the different possible approaches and geometry, one-dimensional (1D) photonic crystals, which are the simplest photonic band gap (PBG) device exploitable to manipulate the emission and absorption properties of lanthanide ions [14–17], are well known to provide good results regarding the nanometric confinement of light [17]. Thus, they can be successfully used to obtain stimulated emission [18]. However, to obtain stimulated emission from erbium-doped 1D photonic crystals, careful and precise tailoring works, both on the geometry and on the involved materials, are required. The systems, in fact, require transparent materials at both excitation and emission wavelengths and the correct configuration to enhance the emission and absorption features of lanthanide ions at all the involved wavelengths [17,19].

The control and reproducibility in the deposition of thin dielectric layers are the most important features in order to fabricate dielectric-based 1D photonic crystals with the correct geometry such that the structure influences the spectroscopic features of the embedded erbium ions at both excitation and emission wavelengths. Processes, such as ion implanting [9], sol–gel [15,20], electron-beam evaporation [21], and sputtering [3,16,17], can be successfully employed for the fabrication of microcavities based on oxide dielectric materials.

Moreover, the real time control of the deposition process is mandatory to permit a precise tailoring of the deposition rate and obtain good uniformity in thickness for dielectric microcavities; in fact, the involved materials present a lower step index than the one that can be obtained using semiconductors [16,17]. On the other hand, to have high reflectivity Bragg reflectors, a fundamental key to reaching a high quality factor is using a great number of alternated layers. This increases the total thickness of the sample and could increase also the possibility to introduce topological imperfection in the sample, reducing the optical quality of the photonic crystal [22].

Other experimental techniques, such as e-beam evaporation with an optical monitoring system for simultaneous reflectance and transmittance measurements during deposition [23], have been demonstrated to be suitable for the fabrication of glass-based 1D photonic crystals. In our case, the requirement to dope each layer with lanthanide ions, with the possibility to change the doping content to optimize the spectroscopic features of the samples, made us choose the RF-sputtering technique.

We have shown that the RF-sputtering is a suitable technique for fabricating dielectric microcavities and to deposit alternating layers of different materials activated by rare-earth ions with controlled refractive index and thickness [16,17]. In these configurations, the absorption of the pump beam and the optical gain-length product are limited owing to the short active regions of the vertical-cavity structures when only the defect layer is activated. It is demonstrated that for an optically pumped organic vertical-cavity laser, in which the whole layer including the Bragg reflectors was doped with a laser dye, the lasing threshold was reduced if compared with a laser with undoped Bragg

reflectors under similar conditions [24], and that RF-sputtering is an optimum technique to fabricate films activated with Er^{3+} ions [16,25,26]. It is also known that PBG structures not only enhance the emission properties of the embedded active systems but can be successfully employed to enhance the absorption feature of the systems [27]. Moreover, the possibility to take advantage of photonic band edges to enhance the density of states of photons is already proved to allow effective output lasing with a low excitation threshold in one-dimensional asymmetric photonic bandgap structure, with a liquid crystal as a defect layer [28]. In the present work, an Er^{3+} doped SiO_2/TiO_2 1D photonic crystal with all TiO_2 and SiO_2 layers doped with Er^{3+} is fabricated using an RF-sputtering technique in different geometrical configurations: samples with different number of layers that compose the Bragg reflectors are compared in order to induce the effect of the geometry of the photonic crystals on the emission. A suitable geometry and pumping scheme are proposed, exploiting the first order of the cavity for the emission and the third order for the pumping, creating the possibility to obtain coherent emission.

2. Materials and Methods

1D Er^{3+} doped dielectric microcavities were fabricated using the RF-sputtering technique. The cavities were fabricated with thin films of SiO_2 and TiO_2, both doped with Er^{3+}. The samples were deposited on SiO_2 and Si substrates. The samples deposited on Si were employed for scanning electron microscopy (SEM) and energy dispersive spectroscopy (EDS) measurements. The samples deposited on SiO_2 were employed for optical and spectroscopic measurements. The substrates were cleaned inside the RF-sputtering deposition chamber by heating at 120 °C for 30 min just before the deposition procedure. The deposition of the films was performed via changing sputtering alternatively between a 15 × 5 cm^2 TiO_2 and 15 × 5 cm^2 SiO_2 targets, on which metallic erbium pieces were placed. The deposition time necessary to reach the appropriate thickness of the Bragg layers, were about 55 min for the silica layer and 1h 30min for titania layers, respectively. The deposition time necessary to reach the appropriate thickness of the silica defect layer, to obtain the cavity resonance centered at 1560 nm, was about 1 h 55 min. The residual pressure before the deposition was 4.5×10^{-5} Pa. During the deposition procedure, the substrates were not heated and the temperature of the sample holder during the deposition was 30 °C. The sputtering occurred with an Ar gas pressure of 0.54 Pa, and the applied RF power was 150 W and 130 W for SiO_2 and TiO_2 targets, respectively. To monitor the thickness of the layers during the deposition, two quartz microbalances, Inficon (Bad Ragaz, Switzerland) instruments thickness monitor model SQM-160, facing toward the two targets were employed. A thickness monitor was calibrated for the two kinds of materials using a long deposition process (24 h of deposition) and directly measuring the thickness of the deposited layer using an m-line apparatus Metricon (Pennington, NJ, USA) [29]. The final resolution on the effective thickness obtained using this quartz microbalance is 0.1nm. More details are available in Reference [17]. The samples were heat-treated at 400 °C for 8 h using a conventional oven.

The compositional analysis was performed using EDS, employing an Oxford mod. INCA PentaFETx3 apparatus (Abingdon, Oxon OX13 5QX, UK). EDS measurements were employed to quantify the erbium content in each layer. SEM was used to analyze the morphology of the multilayer films and thickness of each layer. The cross section of the microcavity was analyzed using an FEG mod. JEOL JSM-7001F (Tokyo 196-8558, Japan) apparatus at 15 kV.

The transmittance measurement of the cavity in the NIR and visible region at a zero-degree incident angle was obtained by using a double beam Varian Cary-5000 spectrophotometer (Agilent Technologies, Santa Clara, CA, USA), which permits performing optical transmittance measurements from 175 to 3300 nm, with a wavelength accuracy of 0.3 nm in all regimes.

The spectroscopic features of the Er^{3+} doped dielectric microcavity were investigated upon excitation at 514.5 nm using the line of an Ar^+ ion laser or a Xenon lamp pass through monochromator with a resolution of 2 nm or a standard tungsten lamp filtered by an interference filter (IF). The spot on the sample surface was 5 mm in diameter for all the excitation options. The angle of excitation

was carefully chosen at 30 degrees to match the third order cavity resonance in case of 514.5 nm excitation. The photoluminescence from the microcavity was detected at 0 degrees from the normal on the samples, with a solid angle of 10^{-1} steradian sr. The emission was dispersed using a 320 mm single-grating monochromator with a resolution of 2 nm. The light was detected by using a Hamamatsu photomultiplier tube (Shizuoka Pref., 430-8587, Japan) and standard lock-in technique. The excitation power of the incident beam was controlled by using neutral density filters. More details about the experimental set up can be found in Reference [17].

3. Results

Three different microcavities were created: in the first one the structure, labelled PC10, consisted of 10 pairs of Er^{3+}-doped, quarter-wavelength alternate SiO_2/TiO_2 layers on each Bragg mirror; in the second one, PC05, had five pairs; and in the third one, called PC07, had 7 pairs. All the structures presented a central defect layer of SiO_2, also doped with Er^{3+}. In Table 1, the geometrical parameters of the three different approaches are reported, which are the number of couples of the Bragg reflectors for the different samples and the optical and spectroscopic features obtained. The quality factor of the cavity, discussed later, was calculated as the ratio between height and full width at half maximum (FWHM) of the first order resonance peak, and is also provided. First-order resonance condition wavelengths, that represent the central wavelengths of the stop band for each sample, as it will be discussed later in detail, are also reported.

Table 1. Geometrical parameters, optical, and spectroscopic features obtained for the three different 1D photonic crystals.

Sample Label	Bragg Grating Geometry	Quality Factor	First-Order Resonance Condition Wavelength (Experimental)	Threshold
PC10	10 pairs	Q = 390 ± 1	1558.5 ± 0.5 nm	30 ± 2 mW
PC05	5 pairs	Q = 110 ± 1	1586.4 ± 0.5 nm	0.6 ± 0.2 mW
PC07	7 pairs	Q = 226 ± 1	1559.2 ± 0.5 nm	4 ± 2 μW

Every sample was deposited at the same time and in the same conditions, both on a SiO_2 substrate, for optical and spectroscopic characterization, and on a Si substrate used for morphological characterization.

Scanning electron microscope (SEM) micrographs of the all Er^{3+} doped 1D dielectric microcavity cross sections are reported in Figure 1a (PC10), 1b (PC05), and 1c (PC07). The dark regions shown in Figure 1 correspond to the SiO_2 layer and the bright regions correspond to the TiO_2 layer. The substrate is located at the bottom of the image and the air on the top. It is possible to identify the defect layer and the two Bragg reflectors.

Energy dispersive spectroscopy (EDS) measurements indicated that the erbium content in all the layers was about 0.2 ± 0.1 mol%. The thicknesses and refractive indices of SiO_2 and TiO_2 thin films were measured using an m-line technique in the 1.5 μm range [16,27] on reference single SiO_2 and TiO_2 films fabricated using the protocol employed for the photonic crystal. The refractive indices for SiO_2 and TiO_2 were 1.44 and 2.2, respectively. The thickness of each layer was monitored during the deposition using the quartz microbalance. The final thickness of each layer measured using SEM microscopy on the Bragg mirror was 270 ± 5 and 170 ± 5 nm for the silica and titania layers, respectively, and a thickness of 540 ± 5 nm for the SiO_2 doped with Er^{3+} defect layer.

The transmittance spectra of the samples are reported in Figure 2. It is possible to identify the stop band for the three samples developed, which were from 1400 nm to 1850 nm, as shown in Figure 2a for the three samples. A sharp peak in the transmission spectra appeared at 1560 nm and corresponds to the cavity resonance related to the Er^{3+}-doped SiO_2 half-wavelength-thick layer inserted between the two Bragg mirrors. Also, it is possible to observe the third order stop band in the visible region, as seen in Figure 2b. The third order of the cavity resonance is also present in the stop band, and appears at 530 nm at a 0 degrees incident angle. At a 30 degrees incident angle, the third-order cavity resonance

was shifted to 514.5 nm. The quality factor of the cavity was calculated as the ratio between wavelength position of the first order resonance peak and his FWHM. The values are reported in Table 1.

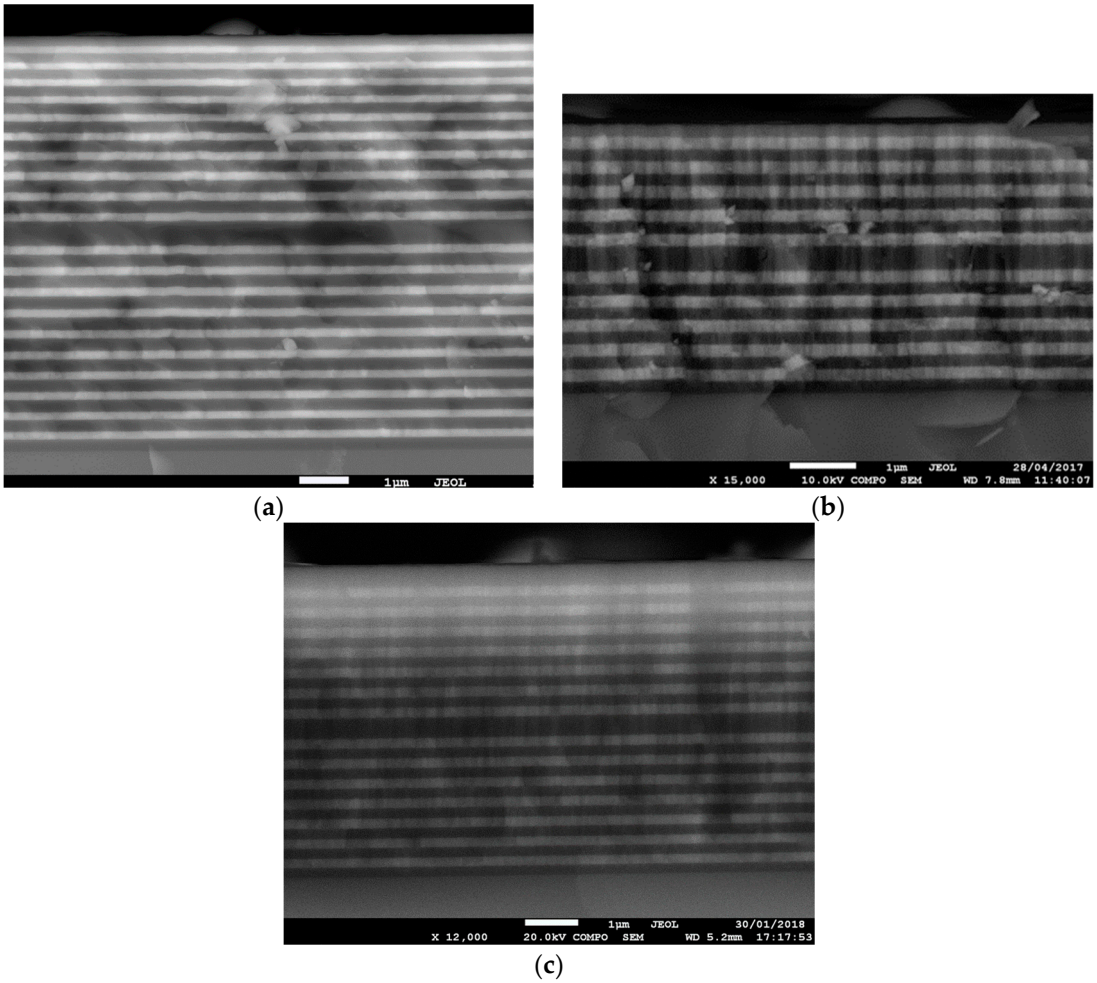

Figure 1. SEM micrograph of the Er^{3+} doped 1D dielectric microcavity cross section: (**a**) sample PC10, (**b**) sample PC05, and (**c**) sample PC07. The bright and dark regions correspond to TiO_2 and SiO_2 layers, respectively. The substrate is located at the bottom of the images and air at the top. All the structures are Er^{3+}-doped with a concentration of 0.2 ± 0.1 mol%.

In Figure 3a, the photoluminescence spectra is reported for the $^4I_{13/2} \rightarrow {}^4I_{15/2}$ transition of the Er^{3+} ions obtained for the PC10 sample at excitation power at 514.5nm of 185 mW and 24 mW with the Ar+ laser. The erbium emission from the microcavity is centered at 1560 nm with FWHM of ≈1.2 ± 0.1 nm that corresponds to the resolution of the detection apparatus in the case of excitation power of 185 mW, while with the 24-mW excitation, the FWHM was equal to 2.4 ± 0.1 nm. The measurement was performed with a detection angle of 0 degrees and an excitation angle of 30 degrees. In Figure 3b, the photoluminescence intensity and the FWHM as a function of the pump power is plotted.

In Figure 4a, the photoluminescence spectra is given for the $^4I_{13/2} \rightarrow {}^4I_{15/2}$ transition of the Er^{3+} ions obtained for the PC07 sample excited under 514.5 nm with the Ar^+ laser (30 mW) and with the tungsten lamp filtered by the interference filter (IF). In the case of laser excitation, the erbium emission from the microcavity was centered at 1535 nm with a FWHM of ≈ 2.2 ± 0.1 nm that corresponds to the resolution of the detection apparatus while with the lamp excitation, the FWHM was equal to 14.5 ± 0.1 nm. The measurement was performed with a detection angle of 0 degrees and an excitation angle of 30 degrees. In Figure 4b, the photoluminescence intensity versus the pump power is given.

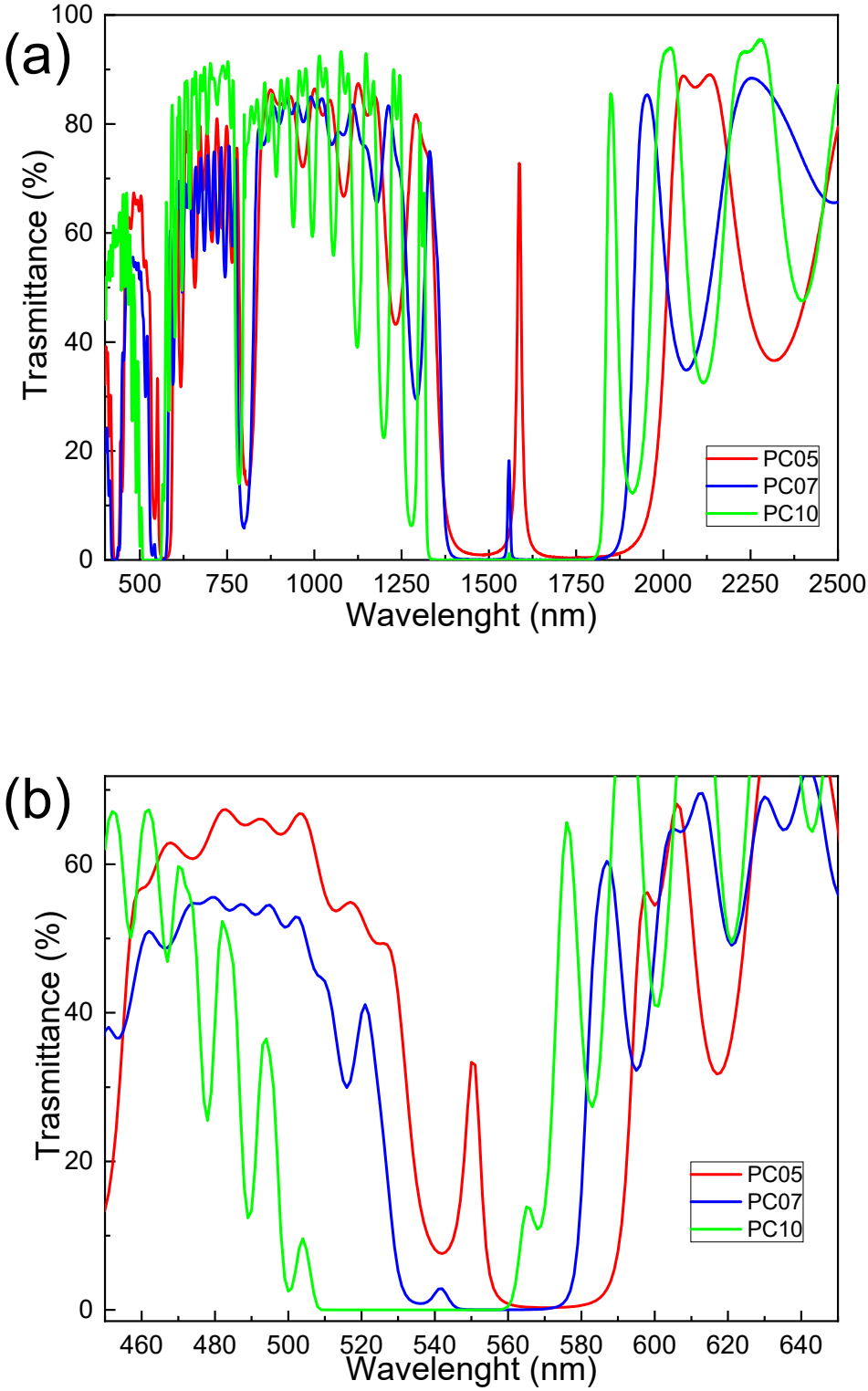

Figure 2. (**a**) Transmission spectrum of the samples PC10 (green line), PC05 (red line), and PC07 (blue line) in the region between 450 nm and 2500 nm. The first order stop band ranged from 1300 nm to 1850 nm. The first order cavity resonances correspond to the sharp maxima centered at 1559.2 nm (PC10), at 1566.8 nm (PC05), and at 1559.9 nm (PC07). The incident light was unpolarized. (**b**) Transmission spectra representing a third order stop band in the visible region between 500 nm to 560 nm with a third order cavity resonance at 536 nm.

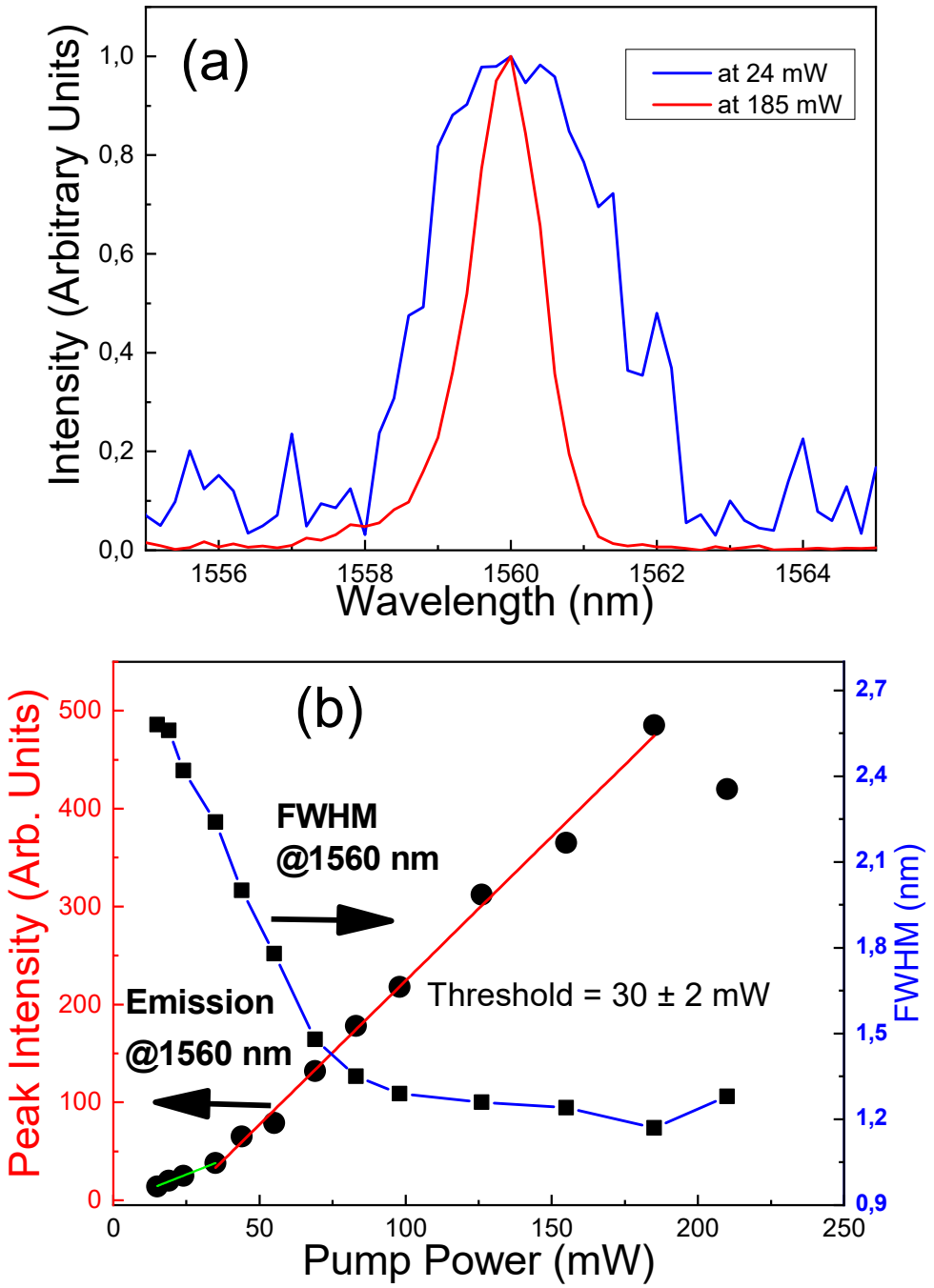

Figure 3. (**a**) $^4I_{13/2} \rightarrow {}^4I_{15/2}$ photoluminescence spectrum of the cavity activated by Er^{3+} ions from the PC10 sample. The emission was recorded at 0 degrees from the normal on the samples upon excitation at 514.5 nm at the input power of 185 mW (red line) and 24 mW (blue line). The excitation angle for both the measurements was 30 degrees. The spectra are normalized. (**b**) $^4I_{13/2} \rightarrow {}^4I_{15/2}$ photoluminescence peak intensity (●) and full width at half maximum (■) at 1560 nm as a function of 514.5 nm pump power with a 0-degree detection angle and a 30-degree excitation angle. Red and green lines are the results of a linear fit while the blue line is a guide for the eyes. Threshold result at 30 mW.

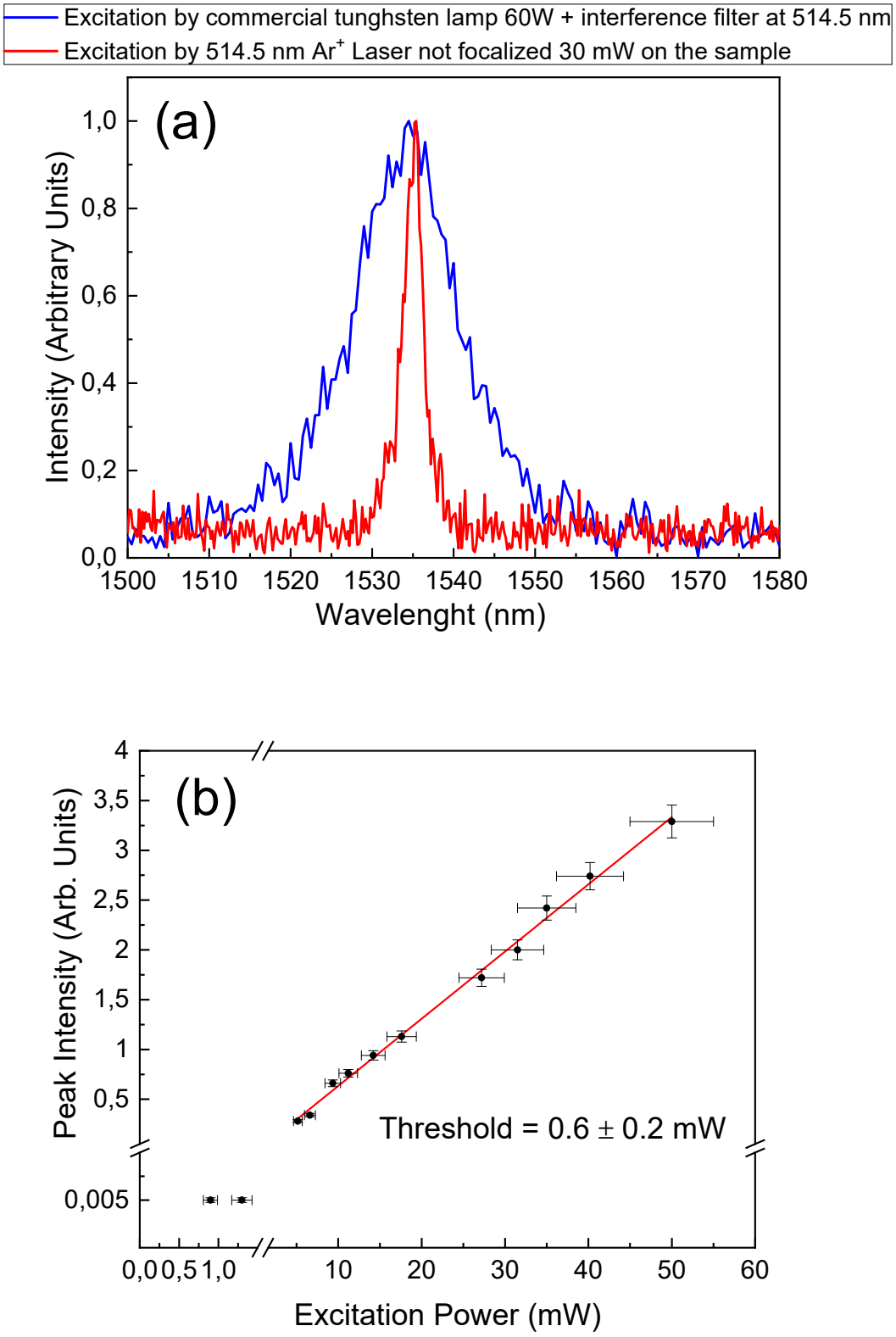

Figure 4. (**a**) $^4I_{13/2} \rightarrow {}^4I_{15/2}$ photoluminescence spectrum of the PC05 sample. The emission was recorded at 0 degrees from the normal on the samples upon excitation at 514.5 nm at the input power of 30 mW (red line) and upon excitation with a conventional tungsten lamp and interference filter centered at 514.5 nm (blue line). The spectra are normalized. (**b**) $^4I_{13/2} \rightarrow {}^4I_{15/2}$ photoluminescence peak at 1535 nm as a function of the 514.5 nm pump power with a 0-degree detection angle and a 30-degree excitation angle. Threshold was obtained at 0.6 mW.

In Figure 5a, the photoluminescence spectrum is given for the $^4I_{13/2} \rightarrow {}^4I_{15/2}$ transition of the Er^{3+} ions obtained for the PC07 sample at an excitation power < 1 mW for the Xenon excitation lamp with a monochromator. The erbium emission from the microcavity was centered at 1535 nm with a FWHM of $\approx 2.1 \pm 0.1$ nm that corresponds to the resolution of the detection apparatus. The measurement was performed with a detection angle of 0 degrees and an excitation angle of 30 degrees. In Figure 5b, the photoluminescence intensity versus the pump power is given. The linear fit of the experimental data intercepts the x-axis at a pump power value of 4 ± 2 μW.

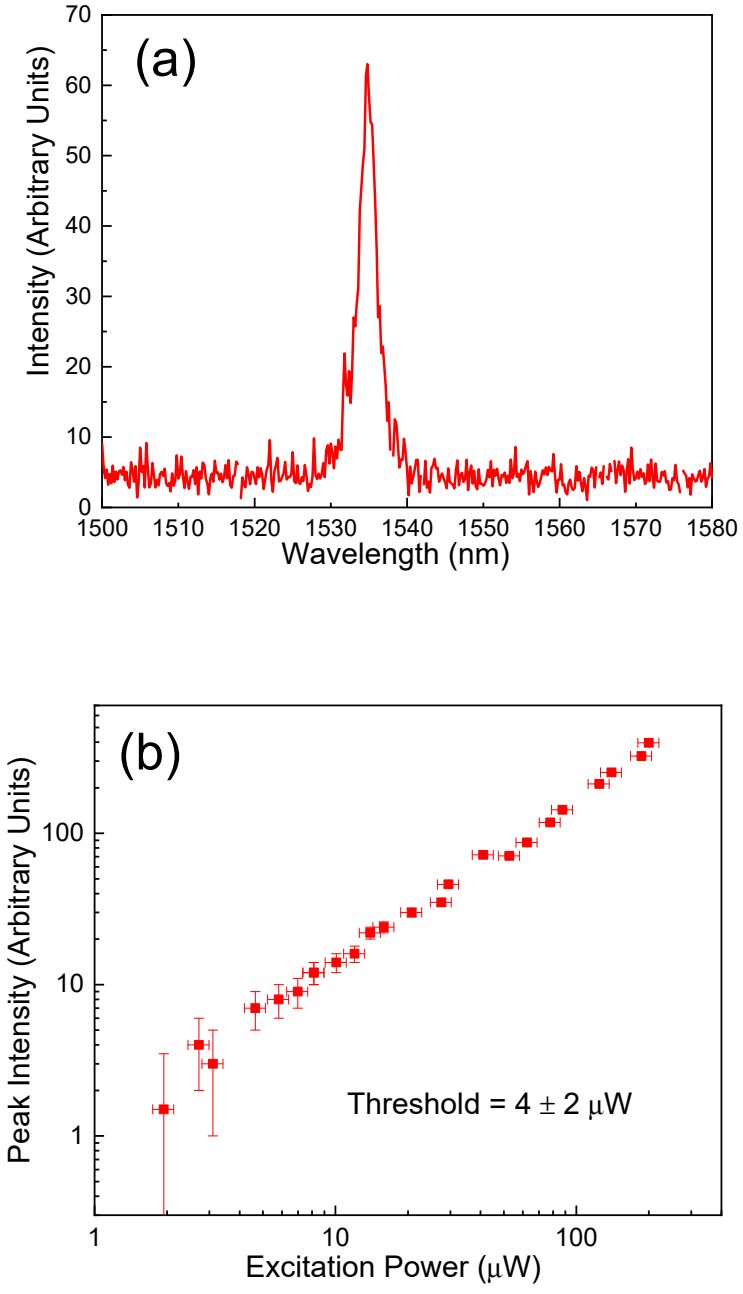

Figure 5. (**a**) $^4I_{13/2} \rightarrow {}^4I_{15/2}$ photoluminescence spectrum from the PC07. The emission was recorded at 0 degrees from the normal on the samples upon excitation at 514.5nm of a Xenon excitation lamp with a monochromator at an input power < 1mW. (**b**) $^4I_{13/2} \rightarrow {}^4I_{15/2}$ photoluminescence peak at 1535 nm as a function of the 514.5 nm pump power with a 0-degree detection angle and a 30-degree excitation angle. Threshold was obtained at 4 μW.

The transmittance spectra is reported in Figure 2a and the data summarized in Table 1 shows that increasing the number of layers in the Bragg reflector increased the quality factor of the structures, but also gave lower transmission values at the resonance peaks. Moreover, the number of defects in the sample increased during the deposition [22]. These facts suggest that an optimization of the number of layers that composed the Bragg grating was necessary to find the best compromise between the high quality factor and the low threshold. It is important to note that the configuration with seven couples for each Bragg reflector exhibits the lower threshold that passed from 30 ± 2 mW for the PC10 sample to 4 ± 2 W for the PC07 photonic crystal.

4. Discussion

One can note that the top layer of sample PC07, the one in direct contact with air, Figure 1c, was made of a half-wavelength layer of lower index SiO_2. This extra thickness enabled one to optimize the reflectance of the top Bragg reflector, taking into account the constructive interference between the Bragg reflector itself, and the SiO_2/air Fresnel reflectance at the interface. From the transmittance spectra of the samples, reported in Figure 2, the stop band for the three developed samples were identified from 1400 nm to 1850 nm, with a sharp peak in the transmission spectra at 1560 nm, corresponding to the cavity resonance. The third order stop band in the visible region was reported in Figure 2b and it was used for exploiting the cavity resonance, not only for the emission, but also for the pumping of the structure. The sample PC10 experienced a high quality factor, 390 ± 1, and defined PBG, with a minimum transmission of 10^{-2}. The sample PC05 experienced a lower quality factor, 110 ± 1, with a higher minimum of transmission, around 2%, but an increased transmission at the resonance condition. From the photoluminescence properties of the three samples, reported in Figure 3a, Figure 4a, and Figure 5a, it is clear that all the samples experienced the narrowing of the FWHM when the pump power was increased. This phenomenon can be explained only by considering stimulated emission as the mechanism involved. The observation of coherent emission in such structures is a huge step in comparison to the old works, where only spontaneous emission was provided [16,17].

An estimation of the threshold of the samples PC10 and PC05, reported in Figures 3b and 4b, respectively, explains the role of the transmission at the resonance condition and of the quality factor in obtaining the decreased threshold. A compromise in obtaining as low a threshold as possible for this system is represented by sample PC07. The transmission characteristics are a compromise between the PC10 and PC05 approach, but the threshold obtained was 4 ± 2μW.

The fabrication of these kind of samples directly on the tip of a fiber is in progress to assess the efficiency of the systems by directly measuring the emitted light in the fiber with an optical spectrum analyzer.

5. Conclusions

Monolithic, fully-doped Er^{3+} dielectric 1D microcavities were fabricated with a defined protocol using an RF-sputtering technique. The structures were created and studied in order to obtain the first-order cavity resonance at 1560 nm at 0 degrees of detection and the third order of the resonance at 514.5 nm at 30 degrees, in order to match, respectively, the emission in the Near Infrared Region of the Er^{3+} ions and the pumping incident field for the excitation of the Er^{3+} ions. Luminescence measurements demonstrated the narrowing of the FWHM of the emission peak intensity at 1560 nm decreasing with the pump power until the spectral resolution of the detection system was 2.7 nm. The emission intensity presented a non-linear behavior with the pump power, and a threshold at about 4μW was observed on the optimized sample composed with Bragg reflectors with seven couples of SiO_2/TiO_2 layers. The results suggested the presence of coherent emission from the sample and further measurements are in progress to define the temporal dynamics of this emission.

Author Contributions: Data curation, F.S., Y.B., A.L., D.R., G.S., S.V., L.Z., M.I., S.T., R.R., G.C.R. and M.F.; Funding acquisition, M.F.; Investigation, C.M. and S.V.; Supervision, M.F. and A.C.; Writing—original draft, C.M.; Writing—review & editing, F.S., Y.B., A.L., D.R., G.S., S.V., L.Z., M.I., S.T., R.R., G.C.R. and A.C.

Funding: This research received no external funding.

Acknowledgments: This research was performed in the framework of the projects COST MP1401 (2014-2018), ERANet-LAC RECOLA (2017-2019), and MiFo -Microcavità Fotoniche Centro Fermi.

Conflicts of Interest: The authors declare no conflict of interest.

References

1. Ferrari, M.; Righini, G.C. *Physics and Chemistry of Rare-Earth Ions Doped Glasses*; Trans Tech Publishers: Pfaffikon, Switzerland, 2008; Chapter 3.
2. Bradley, J.D.B.; Pollnau, M. Erbium-doped integrated waveguide amplifiers and lasers. *Laser Photonics Rev.* **2011**, *5*, 368–403. [CrossRef]
3. Chichibu, S.F.; Ohmori, T.; Shibata, N.; Koyama, T. Dielectric SiO_2/ZrO_2 distributed Bragg reflectors for ZnO microcavities prepared by the reactive helicon-wave-excited-plasma sputtering method. *Appl. Phys. Lett.* **2006**, *88*, 161914-1–161914-3. [CrossRef]
4. Persano, L.; Del Carro, P.; Mele, E.; Cingolani, R.; Pisignano, D.; Zavelani-Rossi, M.; Longhi, S.; Lanzani, G. Monolithic polymer microcavity lasers with on-top evaporated dielectric mirrors. *Appl. Phys. Lett.* **2006**, *88*, 121110-1–121110-3. [CrossRef]
5. Li, Y.; Almeida, R.M. Photoluminescence from a Tb-doped photonic crystal microcavity for white light generation. *J. Phys. D Appl. Phys.* **2010**, *43*, 455101-1–455101-7. [CrossRef]
6. Johnson, C.M.; Reece, P.J.; Conibeer, G.J. Slow-light-enhanced upconversion for photovoltaic applications in one-dimensional photonic crystals. *Opt. Lett.* **2011**, *36*, 3990–3992. [CrossRef] [PubMed]
7. Gonçalves, M.C.; Fortes, L.M.; Almeida, R.M.; Chiasera, A.; Chiappini, A.; Ferrari, M.; Bhaktha, S. Photoluminescence in Er^{3+}/Yb^{3+}-doped silica-titania inverse opal structures. *J. Sol-Gel Sci. Technol.* **2010**, *55*, 52–58. [CrossRef]
8. Snoeks, E.; Lagendijk, A.; Polman, A. Measuring and Modifying the Spontaneous Emission Rate of Erbium near an Interface. *Phys. Rev. Lett.* **1995**, *74*, 2459–2462. [CrossRef]
9. Vredenberg, A.M.; Hunt, N.E.J.; Schubert, E.F.; Becker, P.C.; Jacobson, D.C.; Poate, J.M.; Zydzik, G.J. Erbium implantation in optical microcavities for controlled spontaneous emission. *Nucl. Instrum. Method B* **1993**, *74*, 84–88. [CrossRef]
10. Orignac, X.; Barbier, D.; Min Du, X.; Almeida, R.M.; McCarthy, O.; Yeatman, E. Sol–gel silica/titania-on-silicon Er/Yb-doped waveguides for optical amplification at 1.5 μm. *Opt. Mater.* **1999**, *12*, 1–18. [CrossRef]
11. Hehlen, M.P.; Cockroft, N.J.; Gosnell, T.R.; Bruce, A.J. Spectroscopic properties of Er^{3+}- and Yb^{3+}-doped soda-lime silicate and aluminosilicate glasses. *Phys. Rev. B* **1997**, *56*, 9302–9318. [CrossRef]
12. Strohhöfer, C.; Polman, A. Silver as a sensitizer for erbium. *Appl. Phys. Lett.* **2002**, *81*, 1414–1416. [CrossRef]
13. Portales, H.; Mattarelli, M.; Montagna, M.; Chiasera, A.; Ferrari, M.; Martucci, A.; Mazzoldi, P.; Pelli, S.; Righini, G.C. Investigation of the role of silver on spectroscopic features of Er^{3+}-activated Ag-exchanged silicate and phosphate glasses. *J. Non-Crystalline Solids* **2005**, *351*, 1738–1742. [CrossRef]
14. Rigneault, H.; Amra, C.; Robert, S.; Begon, C.; Lamarque, F.; Jacquier, B.; Moretti, P.; Jurdyc, A.M.; Belarouci, A. Spontaneous emission into planar multi-dielectric microcavities: Theoretical and experimental analysis of rare earth ion radiations. *Opt. Mater.* **1999**, *11*, 167–180. [CrossRef]
15. Jasieniak, J.; Sada, C.; Chiasera, A.; Ferrari, M.; Martucci, A.; Mulvaney, P. Sol–Gel Based Vertical Optical Microcavities with Quantum Dot Defect Layers. *Adv. Funct. Mater.* **2008**, *18*, 3772–3779. [CrossRef]
16. Chiasera, A.; Belli, R.; Bhaktha, S.N.B.; Chiappini, A.; Ferrari, M.; Jestin, Y.; Moser, E.; Righini, G.C.; Tosello, C. High quality factor Er^{3+}-activated dielectric microcavity fabricated by rf sputtering. *Appl. Phys. Lett.* **2006**, *89*. [CrossRef]
17. Valligatla, S.; Chiasera, A.; Varas, S.; Bazzanella, N.; Rao, D.; Righini, G.C.; Ferrari, M. High quality factor 1-D Er^{3+}-activated dielectric microcavity fabricated by RF-sputtering. *Opt. Exp.* **2012**, *20*, 21214–21224. [CrossRef] [PubMed]

18. Settimi, A.; Severini, S.; Sibilia, C.; Bertolotti, M.; Napoli, A.; Messina, A. Coherent control of stimulated emission inside one dimensional photonic crystals: Strong coupling regime. *Eur. Phys. J. B* **2006**, *50*, 379–391. [CrossRef]
19. Gong, Y.; Makarova, M.; Yerci, S.; Li, R.; Stevens, M.J.; Baek, B.; Nam, S.W.; Hadfield, R.H.; Dorenbos, S.N.; Zwiller, V.; et al. Linewidth narrowing and Purcell enhancement in photonic crystal cavitieson an Er-doped silicon nitride platform. *Opt. Exp.* **2010**, *18*, 2601–2612. [CrossRef]
20. Li, Y.; Fortes, L.M.; Chiappini, A.; Ferrari, M.; Almeida, R.M. High quality factor Er-doped Fabry–Perot microcavities by sol–gel processing. *J. Phys. D Appl. Phys.* **2009**, *42*, 205104-1–205104-7. [CrossRef]
21. Ma, G.; Shen, J.; Zhang, Z.; Hua, Z.; Tang, S.H. Ultrafast all-optical switching in one-dimensional photonic crystal with two defects. *Opt. Exp.* **2006**, *14*, 858–865. [CrossRef]
22. Schiller, S.; Goedicke, K.; Reschke, J.; Kirchhoff, V.; Schneider, S.; Milde, F. Pulsed magnetron sputter technology. *Surf. Coat. Technol.* **1993**, *61*, 331–337. [CrossRef]
23. Wu, C.; Zou, Y.; Timofeev, I.; Lin, Y.; Zyryanov, V.Y.; Hsu, J.; Lee, W. Tunable bi-functional photonic device based on one-dimensional photonic crystal infiltrated with a bistable liquid-crystal layer. *Opt. Express* **2011**, *19*, 7349–7355. [CrossRef] [PubMed]
24. Sakata, H.; Takeuchi, H.; Natsume, K.; Suzuki, S. Vertical-cavity organic lasers with distributed-feedback structures based on active Bragg reflectors. *Opt. Exp.* **2006**, *14*, 11681–11686. [CrossRef]
25. Chiasera, A.; Armellini, C.; Bhaktha, S.N.B.; Chiappini, A.; Jestin, Y.; Ferrari, M.; Moser, E.; Coppa, A.; Foglietti, V.; Huy, P.T.; et al. Er^{3+}/Yb^{3+}-activated silica-hafnia planar waveguides for photonics fabricated by rf-sputtering. *J. Non-Crystalline Solids* **2009**, *355*, 1176–1179. [CrossRef]
26. Chiasera, A.; Vasilchenko, I.; Dorosz, D.; Cotti, M.; Varas, S.; Iacob, E.; Speranza, G.; Vaccari, A.; Valligatla, S.; Zur, L.; et al. SiO_2-P_2O_5-HfO_2-Al_2O_3-Na_2O glasses activated by Er^{3+} ions: From bulk sample to planar waveguide fabricated by rf-sputtering. *Opt. Maters.* **2017**, *63*, 153–157. [CrossRef]
27. Sakoda, K. *Optical Properties of Photonic Crystals*; Springer: Berlin, Germany, 2005; Chapter 3.
28. Wang, H.; Lin, J.; Lee, C.; Lee, W. Ultralow-threshold single-mode lasing based on a one-dimensional asymmetric photonic bandgap structure with liquid crystal as a defect layer. *Opt. Lett.* **2014**, *39*, 3516–3519. [CrossRef] [PubMed]
29. Ribeiro, S.J.L.; Messaddeq, Y.; Gonçalves, R.R.; Ferrari, M.; Montagna, M.; Aegerter, M.A. Low optical loss planar waveguides prepared in an organic–inorganic hybrid system. *Appl. Phys. Lett.* **2000**, *77*, 3502–3504. [CrossRef]